*Proc. Natl. Acad. Sci. USA*
Vol. 83, pp. 5136–5140, July 1986
Cell Biology

# Transition from metaphase to anaphase is accompanied by local changes in cytoplasmic free calcium in Pt K2 kidney epithelial cells

(fura-2/digital image processing/mitosis/microtubules/ATP permeabilization)

RAJIV R. RATAN, MICHAEL L. SHELANSKI, AND FREDERICK R. MAXFIELD*

Department of Pharmacology, New York University School of Medicine, 550 First Avenue, New York, NY 10016

*Communicated by Saul Krugman, March 20, 1986*

**ABSTRACT** **We have used a $Ca^{2+}$-sensitive dye, fura-2, to investigate the role of $Ca^{2+}$ during mitosis in Pt K2 epithelial cells. The concentration of cytoplasmic free calcium, $[Ca^{2+}]_i$, increased 2-fold between metaphase and anaphase. Digital image analysis revealed two patterns of $[Ca^{2+}]_i$ localization during anaphase. In half of the anaphase cells, the increase in $[Ca^{2+}]_i$ was greatest in the region near the spindle poles and decreased radially. In the other anaphase cells, there was a ring of high $[Ca^{2+}]_i$ in the cytoplasm, surrounding an area of low $[Ca^{2+}]_i$ in the spindle midzone. Although the reason for the different patterns is not known, peak $[Ca^{2+}]_i$ in both cases was sufficient to maintain a 2- to 6-fold gradient in $[Ca^{2+}]_i$ from the polar region to the midzone. $[Ca^{2+}]_i$ gradients may thus regulate spindle microtubule equilibria and directed chromosome movement during mitosis.**

Orchestration of the complex events of mitosis requires precise mechanisms of spatial and temporal regulation. For example, during anaphase, kinetochore microtubules attached to chromosomes shorten as the chromosomes move to the poles (1). At the same time, interpolar microtubules, which extend from one pole toward the other, lengthen (2, 3). Several observations suggest a role for $Ca^{2+}$ in the control of spindle microtubules. Part of this regulation may be through modulation of a spindle-associated ATPase or kinase. However, there is much evidence that $Ca^{2+}$ may direct assembly and disassembly of microtubules, the structural components of the mitotic spindle fibers, and thereby control spindle dynamics and chromosome movement.

Rapid depolymerization of microtubules is observed when $Ca^{2+}$ is microinjected into the mitotic spindles of echinoderm and mammalian cells (4, 5). During metaphase, microinjection of $Ca^{2+}$ triggers the onset of anaphase (5). Elevation of the concentration of intracellular free $Ca^{2+}$, $[Ca^{2+}]_i$, during anaphase accelerates chromosome-to-pole movement (6, 7). In metaphase, conditions that lower $[Ca^{2+}]_i$ or inhibit $Ca^{2+}$ transport across the plasma membrane delay the transition to anaphase (5, 8). Calmodulin, which sensitizes microtubules to $Ca^{2+}$ (9, 10), is concentrated in the mitotic spindles of cells (11–14).

The mitotic apparatus contains membrane elements that are capable of sequestering and perhaps locally releasing $Ca^{2+}$ (15–17). Lamellar and vesicular membrane elements predominate at the poles while tubular membrane elements are observed to project into the mitotic spindle in close association with kinetochore microtubules (18). Spindle-associated membranes from dividing sea urchin eggs can sequester $Ca^{2+}$ (19), and inositol tris(phosphate)-mediated release of $Ca^{2+}$ during mitosis has been reported (20).

Changes in $[Ca^{2+}]_i$ have been observed during mitosis in Pt K2 rat kangaroo kidney epithelial cells (21) and in sea urchin eggs (22). The release and uptake of $Ca^{2+}$ by intracellular organelles would allow the formation of $Ca^{2+}$ gradients in the cytoplasm (23). We reported that a $[Ca^{2+}]_i$ gradient exists during anaphase in plant cells (24), with $[Ca^{2+}]_i$ highest near the spindle poles. The local increase in $[Ca^{2+}]_i$ in plant endosperm as they progress from metaphase through anaphase is consistent with a role for $Ca^{2+}$ in anaphase microtubule disassembly and directed chromosome movement. To establish the generality of this finding, it is important to demonstrate such a gradient in other cell types.

In this paper, we report a localized increase in $[Ca^{2+}]_i$ as Pt K2 cells progress from metaphase through anaphase. $[Ca^{2+}]_i$ gradients were observed using the highly fluorescent $Ca^{2+}$-sensitive reporter fura-2 (25), which was introduced into the cytoplasm by transient permeabilization with exogenous ATP (26, 27). The observed gradients are consistent with calcium–calmodulin-mediated shortening of kinetochore microtubules in anaphase.

## MATERIALS AND METHODS

**Preparation of Cells.** Pt K2 rat kangaroo kidney epithelial cells were plated at 50–90% confluence in coverslip-bottom tissue culture dishes. Cells were maintained in Dulbecco's modified Eagle's medium (DMEM) with 10% (vol/vol) fetal calf serum, 2 mM L-glutamine, and penicillin/streptomycin in a humidified incubator at 37°C with a 9% $CO_2$/91% air atmosphere. Experiments were performed 2–4 days after plating.

**Fura-2 Loading.** Cells were incubated at 24°C with 250 μM fura-2 and 10 μM ATP in permeabilization buffer (NaCl, 137 mM; KCl, 5 mM; Hepes, 20 mM; glucose, 5.6 mM; EGTA, 15 μM; pH 7.7) for 5 min (26). Permeabilization was stopped by addition of DMEM containing 25 mM Hepes, 10% (vol/vol) fetal calf serum, and penicillin/streptomycin, pH 7.4. Resealed cells were allowed to recover for 20 min at 24°C. They were then placed in incubation medium (NaCl, 150 mM; KCl, 5 mM; $MgCl_2$, 1 mM; $CaCl_2$, 1 mM; Hepes, 20 mM; glucose, 10 mM; pH 7.4) for an additional 40–60 min at 24°C.

**Fluorescence Microscopy.** Measurements were performed on a Leitz Diavert microscope as described (24, 28). Excitation was at 340 nm and 380 nm using a 100-W mercury arc lamp and 10-nm bandpass filters (Oriel, Stamford, CT). The 380-nm filter was paired with a 31.5% transmission quartz neutral density filter (Oriel) to approximately equalize the fluorescence intensities at the two wavelengths. Bleaching of fura-2 is less than 0.05% per second. The time between excitation at each wavelength was approximately 3 sec. A 430-nm long-pass filter was utilized in the emission path. The objective was a 40× Nikon UV-fluor.

**Single-Cell and Multi-Cell Measurements of Mitotic Cells.** Fura-2-loaded cells in metaphase or anaphase were located.

The publication costs of this article were defrayed in part by page charge payment. This article must therefore be hereby marked "*advertisement*" in accordance with 18 U.S.C. §1734 solely to indicate this fact.

Abbreviations: $[Ca^{2+}]_i$, concentration of intracellular (cytosolic) free $[Ca^{2+}]_i$; *I*, intensity of fluorescent emission.

*To whom correspondence should be addressed.

Images of emission with excitation at 340 nm and 380 nm were then recorded at least twice during each stage in the same cell as it progressed through to the completion of mitosis. All cells first examined in metaphase and anaphase completed cell division successfully.

**Conversion of Intensities of Fluorescent Emission into $[Ca^{2+}]$.** As $[Ca^{2+}]$ increases, the 340-nm fluorescence of fura-2 increases, and the 380-nm fluorescence decreases. Conversion of the ratio of the fluorescent intensities at 340 nm and 380 nm ($I_{340}/I_{380}$) to $[Ca^{2+}]_i$ was made by comparison with calibration solutions (25, 28). These solutions contained 500 nM fura-2 in Ca-EGTA buffered solutions prepared as described (28). At 24°C, a dissociation constant of fura-2 for $Ca^{2+}$ of 240 nM was determined.

**Image Analysis.** Fluorescence images at each wavelength were obtained with a Dage-MTI (Michigan City, IN) SIT camera with manual gain and black level control and recorded on a Panasonic NV8030 videotape recorder. Images were digitized from tape using a Gould IP8500 image processor and a Fortel time base corrector. Image processing was performed as described (24). Average $I_{340}/I_{380}$ values were analyzed from distinct regions of each cell as well as whole cells. Determination of the appropriate area of measurement within the cell (e.g., spindle poles) was defined by examination of bright-field images.

**Subcellular Localization of Fura-2.** Cells containing fura-2 were homogenized, and the homogenate was immediately examined using the fluorescence microscope. The homogenate was centrifuged through 0.4 M sucrose buffer at 120,000 × *g* for 15 min at 4°C. The fluorescence in the pellet and supernatant was measured on a 650-10S spectrofluorometer (Perkin–Elmer). $Ca^{2+}$ and EGTA were added sequentially to determine whether the fluorescence was $Ca^{2+}$ sensitive. The concentration of fura-2 in the cytoplasm was determined from the fluorescence in the homogenate, corrected for the total volume of the loaded cells.

**Calmodulin–Fura-2 Interactions.** Calmodulin was dissolved in calibration buffer containing 5 μM fura-2 and equilibrated with buffer by dialysis for 4 hr at 24°C. In separate experiments, $Ca^{2+}$ and EGTA were added to give free $Ca^{2+}$ concentrations of 10 nM and 1 μM. The fura-2 fluorescence excitation spectra over the range 300–400 nm were identical in the calmodulin-supplemented solution and the calmodulin-free solution at both $Ca^{2+}$ concentrations.

**Materials.** Pt K2 cells were obtained from American Type Culture Collection. Tissue culture supplies were from GIBCO. Fura-2 pentapotassium salt was from Molecular Probes (Junction City, OR). ATP (special quality) was from Boehringer Mannheim. Calmodulin (bovine brain) was from Calbiochem–Behring. All other chemicals were from Sigma.

## RESULTS

**Loading of Fura-2 by ATP Permeabilization.** We used ATP permeabilization to introduce the carboxylate form of fura-2 directly into the cytoplasm of Pt K2 cells (26, 27). Twenty to forty percent of the cells in the dish were found to contain fura-2. Loading with the dye appeared to be all or none, and the variability in the signal among loaded cells was small. Using an extracellular fura-2 concentration of 250 μM, the average concentration of dye in loaded cells was 100 μM. Homogenization and subsequent centrifugation of loaded Pt K2 cells demonstrated that 99% of the $Ca^{2+}$-sensitive fluorescence was found in the supernatant. Observation of the crude homogenate as well as the pellet under the fluorescence microscope verified the absence of fura-2 within subcellular organelles. In contrast, cells loaded with fura-2/tetrakis(acetoxymethyl) ester (fura-2/AM) showed punctate fluorescence; homogenization and centrifugation of these cells showed that 44% of the dye was in the pellet.

After loading, cell-associated fluorescence increased 20- to 25-fold with excitation at 340 nm and 20- to 40-fold with excitation at 380 nm in all cells examined. No changes in cellular autofluorescence were observed at 340 nm or 380 nm during mitosis. To determine whether the loading procedure perturbed mitosis, we measured anaphase transit times. We found them to be similar to controls both at 24°C (fura loaded, 23 ± 5 min, vs. controls, 21 ± 4 min, mean ± SEM) and at 37°C (fura loaded, 7.5 ± 1 min, vs. controls, 9 ± 2 min).

**Calcium Levels During Mitosis.** $[Ca^{2+}]_i$ in interphase cells was determined by measuring $I_{340}$ and $I_{380}$ in all areas of the cell excluding the nucleus. We found $[Ca^{2+}]_i$ to be 83 ± 6 nM (mean ± SE, $n$ = 12 cells). The $[Ca^{2+}]_i$ distribution appears homogeneous, except in the nucleus where the $I_{340}/I_{380}$ ratio is lower. We have not included nuclear fluorescence values in the calculation of $[Ca^{2+}]_i$ because precise calibration of fura-2 in the nuclear environment may be difficult.

$[Ca^{2+}]_i$ distribution during mitosis was determined from the 340/380 ratio images. A single cell followed from metaphase through telophase is shown in Fig. 1. Quantitative data on local $[Ca^{2+}]_i$ levels in several mitotic cells are summarized in Table 1.

In metaphase, $[Ca^{2+}]_i$ throughout each half-spindle and the cytoplasm surrounding each half-spindle is 46 ± 10 nM ($n$ = 6 cells). The metaphase plate was excluded from the measurement. $[Ca^{2+}]_i$ in metaphase is significantly lower than $[Ca^{2+}]_i$ in interphase (Table 1). The distribution of $Ca^{2+}$ through most of the metaphase cell is uniform, but a lower $I_{340}/I_{380}$ is found near the metaphase plate (Fig. 1*b*). In the immediate vicinity of the chromosomes, factors unrelated to $[Ca^{2+}]_i$ may affect the $I_{340}/I_{380}$ ratio. In several cells observed in late metaphase, a region of lower $I_{340}/I_{380}$ extends from the metaphase plate into the spindle (Fig. 1*c*). It is unlikely that this enlarged area of low $I_{340}/I_{380}$ is due to an effect of the chromosomes on fura-2, since it is observed before the separation of the chromosomes.

Separation of sister chromatids at the anaphase–metaphase transition is accompanied by a rise in $[Ca^{2+}]_i$ in the spindle polar region to 140 ± 12 nM ($n$ = 11). Within the spindle midzone, $[Ca^{2+}]_i$ is lower than at the poles (Table 1, Figs. 1*e* and 2). Values obtained for the spindle polar region are averages and, therefore, underestimate the peak $[Ca^{2+}]_i$ attained at the spindle pole (Fig. 3). The peak $[Ca^{2+}]_i$ in the polar region is 183 ± 15 nM ($n$ = 11 cells), approximately 2- to 3-fold higher than $[Ca^{2+}]_i$ within the midzone. Peak $[Ca^{2+}]_i$ values represent a 0.5 × 0.5 $\mu m^2$ area at the spindle poles.

Seventeen out of 18 cells examined at 24°C showed localization of $Ca^{2+}$. Six of these cells were not used for quantitative analysis because they became too round during mitosis. As the thickness of the cell increases, contributions from out-of-focus parts of the cell limit our ability to accurately quantify local $[Ca^{2+}]_i$ changes. In similar experiments, four out of five cells examined at 37°C showed localizations of $Ca^{2+}$ during anaphase that were qualitatively similar to those observed at 24°C.

During anaphase, we observed two different patterns of $Ca^{2+}$ localization in the 11 cells included in the quantitative analysis. In six cells, we observed the increase to be greatest in an area corresponding to the spindle poles. Fig. 2 shows an example of this type of highly localized $[Ca^{2+}]_i$. The $Ca^{2+}$ distribution (Fig. 2*d*) is obtained from the ratio of the 340-nm image (Fig. 2*b*) and the 380-nm image (Fig. 2*c*). The individual images show that dye is not concentrated near the poles. In five other cells, a ring of high $[Ca^{2+}]_i$ was observed all around the cell, surrounding the low $[Ca^{2+}]_i$ area in the midzone of the spindle (Fig. 1*e*). In both groups, a gradient is observed between the polar region and the midzone.

Fig. 3 shows the $[Ca^{2+}]_i$ gradient along a line through the cell shown in Fig. 2. The steepness of the gradients observed may actually be underestimated in our experiments since the

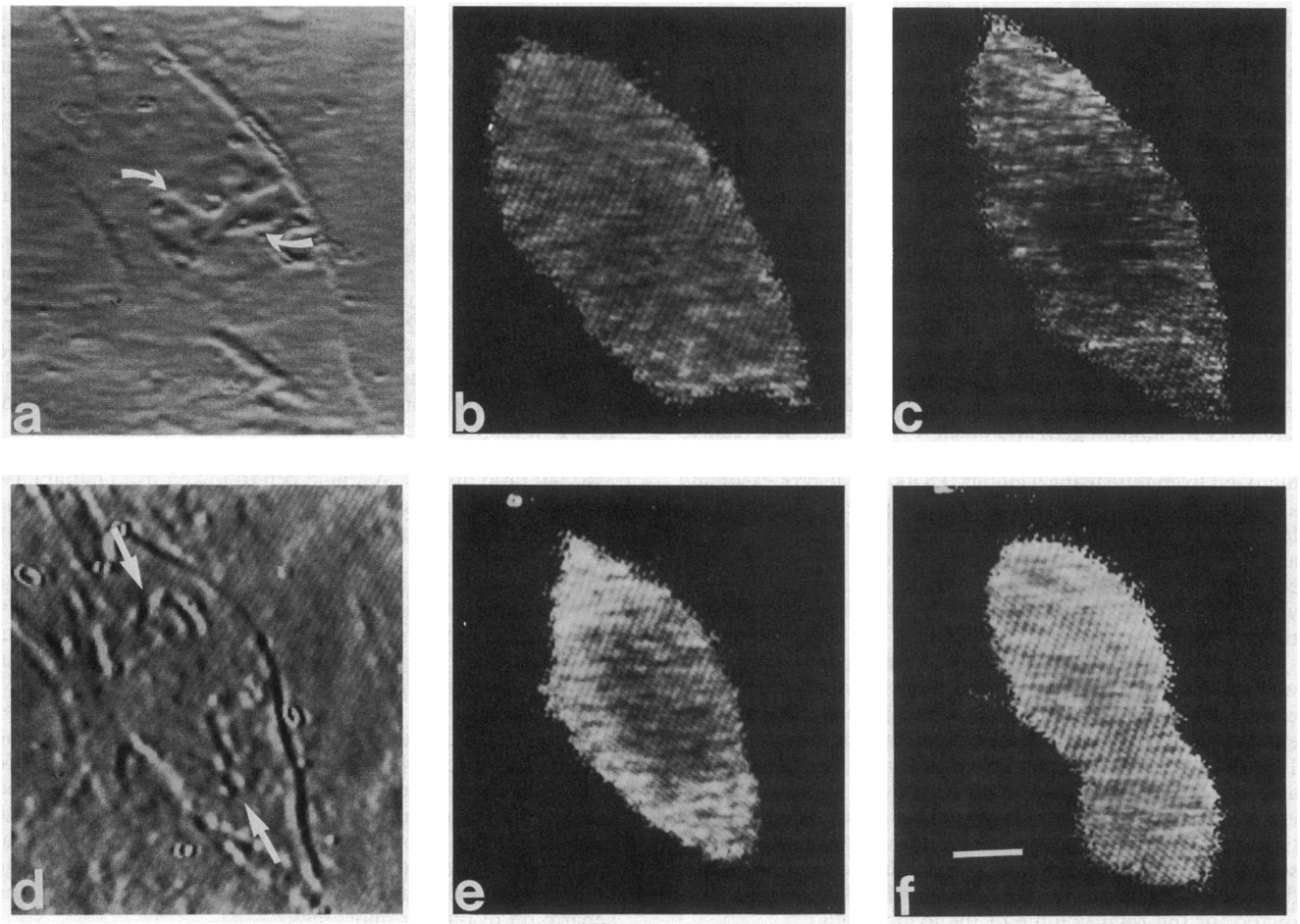


FIG. 1. $[Ca^{2+}]_i$ distribution within a single cell as it proceeds from metaphase to telophase. (*a*) Digitally processed, bright-field image of a Pt K2 cell in early to midmetaphase. Arrows point to the chromosomes aligned at the metaphase plate. (*b*) The $[Ca^{2+}]_i$ distribution in the same cell, with brightness proportional to $[Ca^{2+}]_i$. The average $[Ca^{2+}]_i$, excluding the metaphase plate, is 40 nM. Fluorescent images with excitation at 340 nm and 380 nm were recorded on videotape and digitized (512 × 512 pixels, 256 grey levels). The mean background intensity from around the cells was subtracted from each image. The background-corrected 340-nm image was divided by the background-corrected 380-nm image. A fluorescence-intensity threshold was set in the 380-nm image before division to exclude noncellular regions from the determination of the ratio image. The use of a threshold excludes some thin parts of the cell from the ratio calculation, but it has no effect on $I_{340}/I_{380}$ values within the remainder of the cell. The resultant $I_{340}/I_{380}$ ratio image was redisplayed according to a calibration curve as an image of $[Ca^{2+}]$ at each point in the cell. The time at which this image was observed was defined as 0 min. (*c*) The $[Ca^{2+}]_i$ distribution of the same cell in late metaphase, with brightness proportional to $[Ca^{2+}]_i$. The average $[Ca^{2+}]_i$, excluding the metaphase plate is 44 nM. A region of low $[Ca^{2+}]_i$ is expanding outward from the metaphase plate. Time, 85 min. (*d*) Digitally processed, bright-field image of the same cell in anaphase. Arrows point to the mitotic spindle poles. (*e*) $[Ca^{2+}]_i$ distribution in anaphase. A ring of high $[Ca^{2+}]_i$ surrounds the area of lower $[Ca^{2+}]_i$ in the midzone. Peak $[Ca^{2+}]_i$ at the mitotic spindle poles (arrows in *d*) is 240 nM, and average $[Ca^{2+}]_i$ within the midzone is 92 nM. Whole-cell $[Ca^{2+}]_i$ in anaphase is 125 nM. Time, 110 min. (*f*) Distribution of $[Ca^{2+}]_i$ in telophase. Whole-cell $[Ca^{2+}]_i$ is 120 nM. Time, 123 min. (Bar = 5 $\mu$m.)

presence of fura-2, a diffusible $Ca^{2+}$ buffer, would be expected to diminish $[Ca^{2+}]_i$ gradients. Furthermore, the images contain intensity from out-of-focus elements, which would also contribute to the underestimation of $Ca^{2+}$ gradients. Qualitatively, there were no significant differences in the $[Ca^{2+}]_i$ measured at the spindle poles and the midzone in the two groups, and both proceeded through mitosis normally. Whole-cell $Ca^{2+}$ does not change significantly from early to late anaphase. However, a small increase (approximately 10%) in average $[Ca^{2+}]_i$ within the midzone is observed. The low $[Ca^{2+}]_i$ in the midzone persists until the daughter nuclei begin to reform when $Ca^{2+}$ becomes evenly distributed throughout the cytoplasm (Fig. 1*f*). Whole-cell $[Ca^{2+}]_i$ does not change as cells progress from anaphase (90 ± 11 nM, $n$ = 11) through telophase (95 ± 15 nM, $n$ = 11).

## DISCUSSION

We have shown that remarkably steep and stable gradients of $[Ca^{2+}]_i$ exist in mammalian cells during anaphase. Similar gradients were observed during anaphase in a plant cell (24). The region of high $[Ca^{2+}]_i$ includes the mitotic spindle poles and corresponds to a region of high calmodulin concentration during anaphase. A region of low $[Ca^{2+}]_i$ is centered in the interchromosomal region and extends outward beyond the chromosomes. Thus, the kinetochore microtubules are exposed to the steepest part of the $[Ca^{2+}]_i$ gradient. The steepness of the $[Ca^{2+}]_i$ gradient is shown in Fig. 3. Maintenance of this gradient for several minutes in the presence of 100 $\mu$M fura-2 shows that the cell has high capacity systems for the local release and removal of cytoplasmic calcium. Membrane-bound organelles, which might release and sequester $Ca^{2+}$, have been found within the mitotic apparatus (19).

Several types of evidence suggest a critical role for $Ca^{2+}$ in regulating mitosis, particularly through the control of microtubule equilibria. It has been proposed that the rate of shortening of kinetochore microtubules is the rate limiting factor in chromosome motion to the poles (29). The high $[Ca^{2+}]_i$ and calmodulin concentration would favor disassem

Table 1. $[Ca^{2+}]_i$ in mitotic and interphase Pt K2 cells

| Stage* | Region | Average $[Ca^{2+}]_i$ |
|---|---|---|
| Interphase | Cytoplasm, excluding nucleus | 83 ± 6 nM (12)† |
| Metaphase | Whole cell, excluding metaphase plate‡ | 46 ± 10 nM (6) |
| Anaphase | Whole cell | 90 ± 11 nM (11) |
| | Spindle poles (2 × 2 $\mu m^2$, area) | 140 ± 15 nM (11) |
| | Spindle midzone§ | 74 ± 12 nM (11) |
| Telophase | Cytoplasm, excluding nuclear region | 95 ± 15 nM (11) |

*Cells were assigned to stages of mitosis by observation in bright-field microscopy as described (21).
†All values are mean ± SEM with the number of cells used for the observation in parentheses.
‡The area at the metaphase plate usually showed a lower $I_{340}/I_{380}$ value, perhaps as a result of local effects at the chromosomes.
§Measured in a rectangular area between the separating chromatids.

bly of kinetochore microtubules selectively at the polar ends. Similarly, the growing area of low $[Ca^{2+}]_i$ in late metaphase/early anaphase may be necessary to stabilize kinetochore microtubules in the region near the chromosomes.

As the kinetochore microtubules are shortening, the polar microtubules are growing. Since these polar microtubules also have their minus ends in the region of high calcium (30), there must be a mechanism for separately regulating the two types of microtubules. One such mechanism would involve a differential sensitivity of the two types of microtubules to calcium–calmodulin. In mammalian fibroblasts and higher plant cells, it has been found that calmodulin extends into the mitotic spindle with a distribution that closely parallels the kinetochore microtubules (13, 14). If calmodulin preferentially associates with the kinetochore microtubules, this could account for the difference in the behavior of the two types of microtubules in regions of high $[Ca^{2+}]_i$.

Although microtubule disassembly may regulate the rate of chromosome motion, other molecules may actually be responsible for the force generation. Since the nature of such force generating molecules has not been firmly established, the possible role of $[Ca^{2+}]_i$ in regulating the force generation cannot be assessed.

Several potential artifacts must be considered in studies of $[Ca^{2+}]_i$ using fura-2. Some fura-2 fluorescence could be from dye in organelles or bound to macromolecules. The diffuse pattern of fluorescence and the subcellular fractionation of loaded cells indicate this is not a problem for cells loaded by reversible ATP permeabilization. (We did observe a punctate pattern of fluorescence and sedimentable fura-2 in homogenates when cells were loaded at 37°C using fura-2/AM, a permeant ester of fura-2.) We also verified that high concentrations of calmodulin do not affect fura-2 fluorescence at low or high $[Ca^{2+}]_i$ and that fura-2 does not bind significantly to calmodulin. Thus, the localization of calmodulin in the spindle should not alter the ability of fura-2 to measure $[Ca^{2+}]_i$.

The average concentration of fura-2 in cells permeabilized with ATP was approximately 100 $\mu$M. As a $Ca^{2+}$ chelator, fura-2 could act to reduce the magnitude of $[Ca^{2+}]_i$ changes without necessarily affecting the progress of mitosis. This type of buffering effect could explain why a previous study in our laboratory using quin-2 (approximately 1 mM inside the cell) found no increase in whole-cell $[Ca^{2+}]_i$ during anaphase in Pt K2 cells (21).

Artifacts might also arise if fura-2 fluorescence does not accurately reflect $[Ca^{2+}]_i$. Fura-2 represents a significant improvement over quin-2 in its increased selectivity for $Ca^{2+}$ over $Mg^{2+}$ and heavy metals. However, calibration of dye fluorescence was done in a buffer that approximates the intracellular environment in terms of pH, $Mg^{2+}$, and ionic strength. Factors such as microviscosity and binding of the dye to proteins, which could alter the response of the dye to $[Ca^{2+}]_i$, are more accurately accounted for by an in-cell calibration. A study has indicated that plots of $I_{340}/I_{380}$ vs. $[Ca^{2+}]$ are not greatly different in the intact smooth muscle cell as compared to fura-2 in solution (31).

This study demonstrates the existence of localized changes in $[Ca^{2+}]_i$ in Pt K2 cells as they progress from metaphase to anaphase. These results are consistent with the following model for $Ca^{2+}$-regulated events during mitosis: In metaphase, the low $[Ca^{2+}]_i$ would tend to stabilize the spindle. As a cell goes from metaphase to anaphase, membrane-limited compartments would actively take up $Ca^{2+}$ and locally release it at the spindle poles. This $Ca^{2+}$, acting through

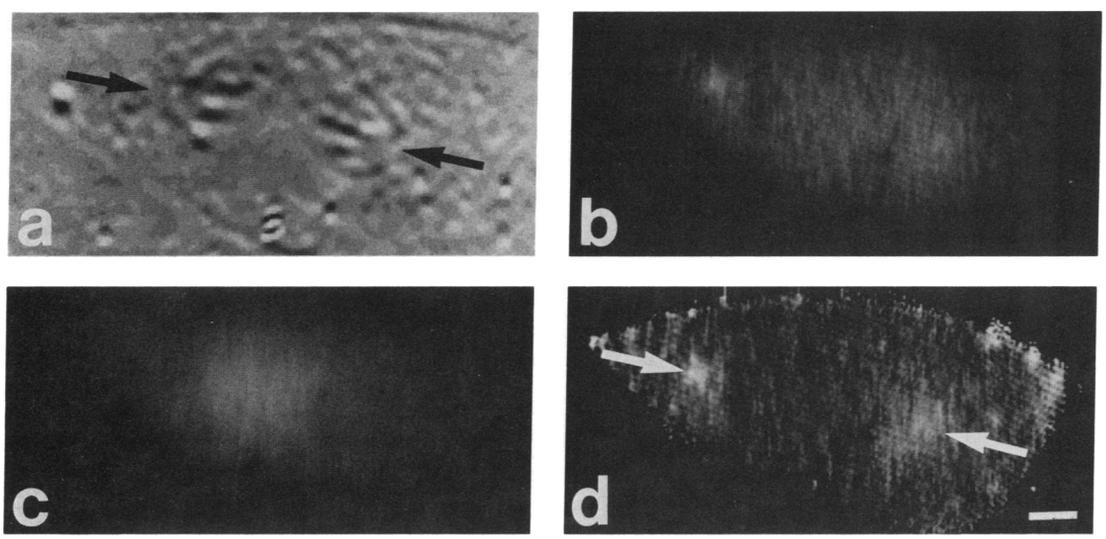


FIG. 2. Fura-2 fluorescence images of a Pt K2 cell in anaphase depicting locally high calcium at the spindle poles. (*a*) Digitally processed, bright-field image of a cell in anaphase. Arrows point to the mitotic spindle poles. (*b* and *c*) Background-corrected fluorescence images of the same cell with excitation at 340 and 380 nm after loading with fura-2. The images were corrected for background intensities as described in Fig. 1. Regions corresponding to the cell were identified using a threshold intensity in the 380-nm image, and $[Ca^{2+}]$ was calculated from $I_{340}/I_{380}$ value as in Fig. 1. This image of calcium distribution was then redisplayed (*d*). For this cell, peak $[Ca^{2+}]_i$ at the spindle poles (arrows) is 220 nM. The average $[Ca^{2+}]_i$ within the spindle midzone is 88 nM. (Bar = 5 $\mu$m.)

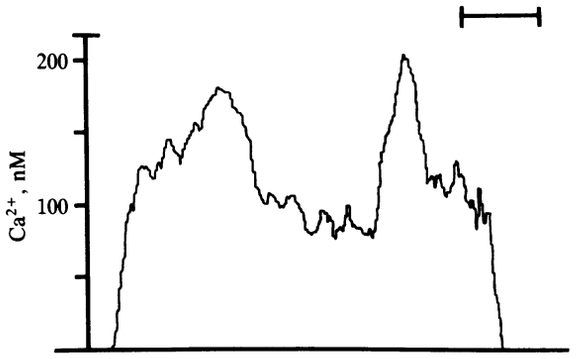


FIG. 3. Profile of the spatial variation in $[Ca^{2+}]_i$ along a vector in the anaphase Pt K2 cell. The $[Ca^{2+}]_i$ along a line through the cell shown in Fig. 2 is displayed. The vector was drawn from one cell boundary to the other passing through both spindle poles and through the spindle midzone. To reduce random noise in single pixels, the image in Fig. 2*d* was convolved with a 31 × 31 gaussian kernel prior to calculation of $[Ca^{2+}]_i$ along this line. (Bar = 10 $\mu$m.)

calmodulin, causes kinetochore microtubules to shorten at the poles, thus allowing the chromosomes to move toward the poles. The lower $[Ca^{2+}]_i$ in the interchromosomal region allows the polar microtubules to elongate and, thereby, to facilitate or drive separation of the poles. Further work is required to identify the force-generating mechanism(s) of the mitotic spindle and to establish the precise role of local $[Ca^{2+}]_i$ gradients.

We acknowledge helpful discussions with Dr. C. Keith, B. Kruskal, A. Bush, and D. Yamashiro. We thank H. Diaz for expert technical assistance. R.R.R. was supported by Grant GM 07308 from the Medical Scientist Training Program of the National Institutes of Health. This work was funded by Grants GM 34770 to F.R.M. and NS 15076 to M.L.S. from the National Institutes of Health.

1. Inoue, S. & Sato, H. (1967) *J. Gen. Physiol.* **50,** 259–292.
2. McIntosh, J. R., McDonald, K. L., Edwards, M. K. & Ross, B. M. (1979) *J. Cell Biol.* **83,** 428–442.
3. McDonald, K. L., Edwards, M. K. & McIntosh, J. R. (1979) *J. Cell Biol.* **83,** 443–461.
4. Kiehart, D. P. (1981) *J. Cell Biol.* **88,** 604–617.
5. Izant, J. G. (1983) *Chromosoma* **88,** 1–10.
6. Cande, W. Z. (1981) in *International Cell Biology*, ed. Schweiger, H. G. (Springer, Berlin), pp. 382–391.
7. Hauser, M. & Beier, A. M. (1980) *Eur. J. Cell Biol.* **22,** 313.
8. Hepler, P. K. (1985) *J. Cell Biol.* **100,** 1363–1368.
9. Marcum, J. M., Dedman, J. R., Brinkley, B. R. & Means, A. R. (1978) *Proc. Natl. Acad. Sci. USA* **75,** 3771–3775.
10. Keith, C. H., Dipaola, M., Maxfield, F. R. & Shelanski, M. L. (1983) *J. Cell Biol.* **97,** 1918–1924.
11. Welsh, M. J., Dedman, J. R., Brinkley, B. R. & Means, A. R. (1978) *J. Cell Biol.* **81,** 624–634.
12. Zavortink, M., Welsh, M. J. & McIntosh, J. R. (1983) *Exp. Cell Res.* **149,** 375–385.
13. Willingham, M. C., Wehland, J., Klee, C. B., Richert, N. D., Rutherford, A. V. & Pastan, I. H. (1983) *J. Histochem. Cytochem.* **31,** 445–461.
14. Vantard, M., Lambert, A. M., De Mey, J., Picquot, P. & Van Eldik, L. J. (1985) *J. Cell Biol.* **101,** 488–499.
15. Wick, S. M. & Hepler, P. K. (1980) *J. Cell Biol.* **86,** 500–513.
16. Wolniak, S. M., Bart, K. M. & Hepler, P. K. (1983) *J. Cell Biol.* **96,** 598–605.
17. Schatten, G. & Schatten, H. (1982) *Cell Biol. Int. Rep.* **6,** 717–724.
18. Hepler, P. K. (1980) *J. Cell Biol.* **86,** 490–499.
19. Silver, R. B., Cole, R. D. & Cande, W. Z. (1980) *Cell* **19,** 505–516.
20. Sillers, P. & Forer, A. (1985) *Cell Biol. Int. Rep.* **9,** 275–282.
21. Keith, C. H., Maxfield, F. R. & Shelanski, M. L. (1985) *Proc. Natl. Acad. Sci. USA* **82,** 800–804.
22. Poenie, M., Alderton, J., Tsien, R. Y. & Steinhardt, R. A. (1985) *Nature (London)* **315,** 147–149.
23. Rose, B. & Lowenstein, W. R. (1975) *Nature (London)* **254,** 250–252.
24. Keith, C. H., Ratan, R., Maxfield, F. R., Bajer, A. & Shelanski, M. L. (1985) *Nature (London)* **316,** 848–850.
25. Grynkiewicz, G., Poenie, M. & Tsien, R. Y. (1985) *J. Biol. Chem.* **260,** 3440–3450.
26. Gomperts, B. D. (1983) *Nature (London)* **306,** 64–66.
27. Heppel, L. A., Weisman, G. A. & Friedberg, I. (1985) *J. Membr. Biol.* **6,** 189–196.
28. Kruskal, B., Keith, C. H. & Maxfield, F. R. (1984) *J. Cell Biol.* **99,** 1162–1167.
29. Inoue, S. (1982) *J. Cell Biol.* **91,** 131s–147s.
30. Euteneuer, U., Jackson, W. T. & McIntosh, J. R. (1982) *J. Cell Biol.* **94,** 644–653.
31. Williams, D. A., Fogarty, K. E., Tsien, R. Y. & Fay, F. S. (1985) *Nature (London)* **318,** 558–561.